NANO MICRO small

DOI: 10.1002/smll.200500165

High-Yield Synthesis of Single-Crystal Nanosprings of ZnO**

*Pu Xian Gao and Zhong Lin Wang**

Zinc oxide, an important member in the II–VI group semiconductors, has profound applications in optics, optoelectronics, sensors, and actuators due to its semiconducting, piezoelectric, and pyroelectric properties.[1–4] Structurally, wurtzite-structured ZnO has 13 fast growth directions: [0001], $<01\bar{1}0>$, and $<2\bar{1}\bar{1}0>$; 12 lower energy facets, $\{01\bar{1}0\}$ and $\{2\bar{1}\bar{1}0\}$; as well as a pair of polar surfaces, {0001}.[5] These structural features allow ZnO to exhibit a group of unique and novel nanostructures,[6,7] such as nanowires,[8,9] nanotubes,[10] nanobelts,[11] nanocombs,[12] nanosprings,[13] nanorings,[14] nanobows,[15,16] nanojunction arrays,[17,18] nanopropeller arrays,[19] nanoplatelets,[20] and nanodiskettes.[21] The diversity and splendid nanostructures of ZnO could confer on it the same importance as that of carbon nanotubes for exploring nanoscale phenomena and devices. The single-crystal nanorings and nanosprings of ZnO, for example, are potential candidates for building semiconducting and piezoelectric resonators, actuators, and sensors for chemical and biological detection. It is necessary, as the first step, to synthesize nanosprings at high yield.

However, the formation of nanosprings relies on nanobelts that are dominated by the {0001} polar surfaces, which have higher energy than the $\{01\bar{1}0\}$ and $\{2\bar{1}\bar{1}0\}$ planes, and are energetically unfavorable to form during growth. An energy barrier has to be overcome by controlling growth kinetics to form polar-surface-dominated nanosprings. Therefore, the yield of nanosprings was lower than 5%,[13] greatly limiting their application in electromechanical-coupled nanodevices. In this paper, we report the successful manipulation of growth kinetics to synthesize single-crystal ZnO nanorings at a high yield of more than 50%. This work pushes ZnO nanosprings from a scientific phenomenon to a practical material for carrying out a wide range of physical, mechanical, chemical, and biological experimental studies. The rational control of high-yield synthesis of piezoelectric ZnO nanosprings could open a new era in ZnO-based electromechanical-coupled nanodevices.

[*] P. X. Gao, Prof. Z. L. Wang
School of Materials Science and Engineering
Georgia Institute of Technology
Atlanta, GA 30332-0245 (USA)
Fax: (+1) 404-894-8008
E-mail: zhong.wang@mse.gatech.edu

[**] Thanks are expressed to the NASA Vehicle Systems Program and the Department of Defense Research and Engineering (DDR&E) for their financial support, to the Defense Advanced Research Projects Agency, and to the NSF NIRT programs.

Our synthesis is based on a high-temperature solid–vapor process. In comparison to our previous experiments,[22] we did not introduce any dopants, such as Li or In ions, in the source materials. The key is to control growth kinetics. A systematic characterization of the as-grown nanostructures at different deposition areas of different local growth temperature was conducted by scanning electron microscopy (SEM) to examine the morphology and chemical composition. In a region of 500–600 °C, it was observed that high yield of nanosprings was successfully achieved on a polycrystalline alumina substrate. This type of experiment was repeated over five times.

Among the as-synthesized products, the most frequently found nanostructure is a single-crystal nanospring. Figure 1a displays a typical low-magnification SEM image of the as-grown ZnO nanosprings, with a yield of $>50\,\%$, distributed densely and uniformly on a polycrystalline Al_2O_3 substrate.

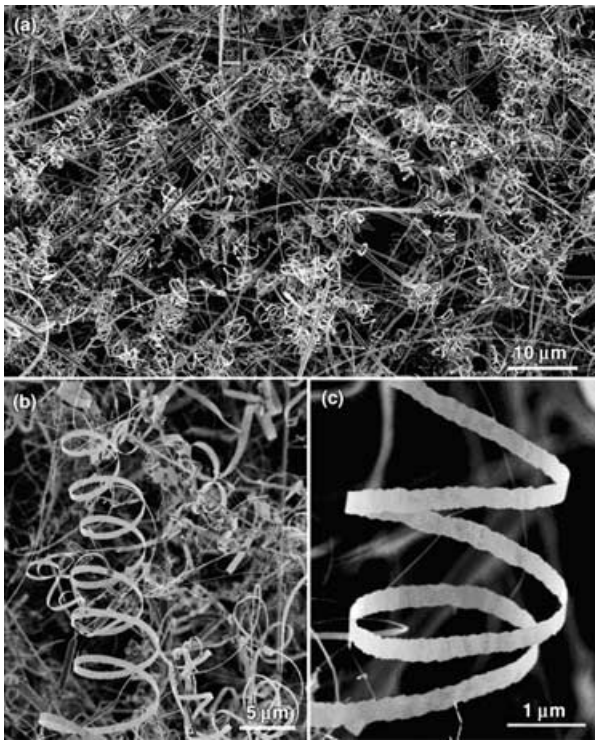

Figure 1. a) A low-magnification SEM image of the as-synthesized ZnO sample, demonstrating a predominance of nanosprings in the product. b,c) Enlarged SEM images showing the detailed morphology of individual nanosprings.

The typical dimensions of an individual nanospring are 1–4 μm in diameter, 1–3 μm in pitch distance, and tens of micrometers long (Figure 1b). The coiled nanobelt, from which the nanospring is formed, is tens of nanometers in thickness and ≈0.2–1 μm in width. Some of the nanosprings tend to be entangled with each other, but the majority of them are separated and randomly located on the substrate. The high-magnification SEM image in Figure 1c reveals the surface morphology of an individual ZnO nanospring. The nanospring has a width of about 300 nm, a diameter of ≈3 μm, while the pitch distance ranges from 1–3 μm. Both edges of the coiling nanobelt across its width are of a zigzag nature. The larger surfaces are rather smooth in comparison to the side edges. Both right-handed and left-handed chiralities have been found.

The structure of the nanosprings is characterized by transmission electron microscopy (TEM). A nanospring of diameter ≈5 μm is projected from the top view in Figure 2a, where a circular shaped looping is clearly revealed. Figure 2b is a projected image of a nanospring from the side view. The projected nanospring has a width of ≈250 nm, a pitch distance of ≈4 μm, and a diameter of around 4 μm. Figure 2c shows a magnified TEM image of the nanospring, where the bending contours are clearly shown, indicating its single-crystal structure. A high-resolution TEM image of the nanoring is given in Figure 2d. The electron diffraction pattern in the inset of Figure 2d shows that the nanobelts forming the nanosprings are dominated

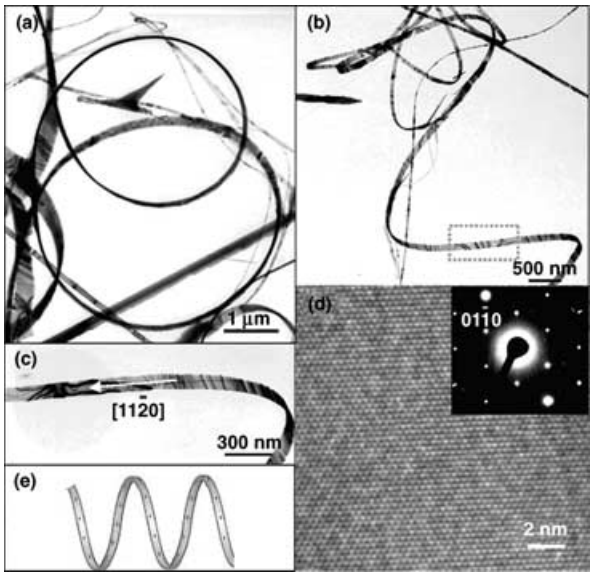

Figure 2. TEM images showing top (a) and side (b) views of a ZnO nanospring. c) A magnified TEM image presents the single-crystal structure of the nanospring and the growth direction of the nanobelt. d) A high-resolution TEM image and the corresponding electron diffraction pattern recorded from the nanobelt coiling into a nanospring. The image shows that the nanobelt is dominated by the {0001} polar surfaces, its growth direction $[2\bar{1}\bar{1}0]$, and its dislocation-free volume. e) A schematic model of the polar-surface-dominated nanospring.

by the {0001} polar surfaces and grow along the $[11\bar{2}0]$ direction (*a* axis).

Structurally, the wurtzite-structured ZnO can be described as a number of alternating planes composed of tetrahedrally coordinated O^{2-} and Zn^{2+} ions that are stacked alternatively along the *c* axis. The oppositely charged ions produce positively charged Zn(0001) and negatively charged $O(000\bar{1})$ polar surfaces, resulting in a normal dipole moment and spontaneous polarization along the *c* axis as well as a divergence in surface energy. During the synthesis, the high growth temperature and inert gas environment in

the growth chamber may greatly limit the adsorption of foreign molecules on the surface. If the ionic charges on the surface are uncompensated, the nanobelt tends to fold over in order to reduce the electrostatic energy.[13] If the nanobelt is rolled in a uniradial manner, loop-by-loop, the repulsive force between the charged surfaces stretches the nanospring, while the elastic deformation force pulls the loops together; the balance between the two leads to the formation the nanospring/nanohelix (Figure 2e).[22]

The other types of frequently observed structures are nanoloops, nanospirals, or unclosed nanorings. Figures 3a, b and c display three typical configurations of nanoloops,

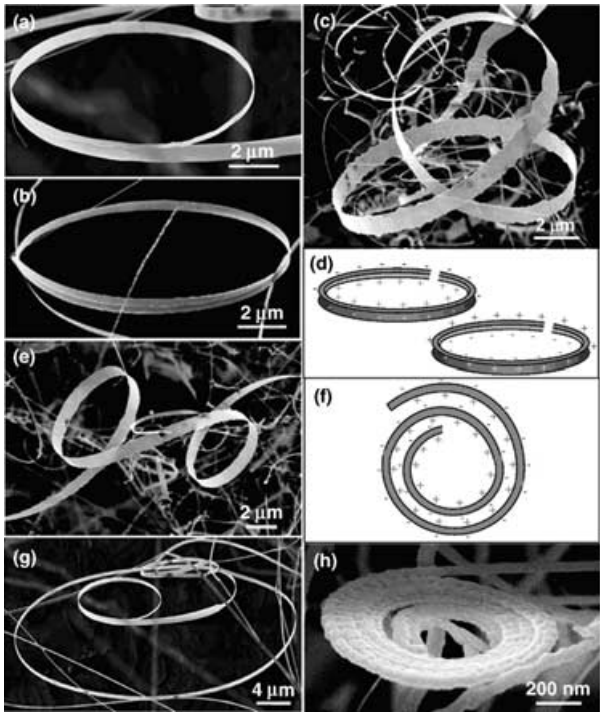

Figure 3. a–c) SEM images of ZnO nanoloops (or nanorings) formed at the ends of nanobelts. d) Schematic models of the nanoloop formation, where "+" indicates the Zn^{2+}-terminated surface and "–" indicates the O^{2-}-terminated surface. e) An SEM image of "twin" nanoloops corresponding to the model shown in (d). f) Schematic model of the formation of a nanospiral, and g,h) show two corresponding experimental images.

which are formed by rolling the nanobelts circularly. TEM imaging and electron diffraction analysis indicate that the nanobelts forming the nanoloops are dominated by the {0001} large flat surfaces and grow along $[10\bar{1}0]$ (Figure 4). The formation of the nanoloops reduces the electrostatic energy created by the polar charges on the {0001} surfaces. In one case, if the inner surface of the loop is Zn^{2+}-terminated and the outer surface is O^{2-}-terminated, from an energy point-of-view, this should be identical to having the reverse case in which the inner surface is O^{2-}-terminated and the outer surface is Zn^{2+}-terminated, as shown in Figure 3d. Experimental evidence of such a case is given in Figure 3e, in which the two rings have opposite charges on the

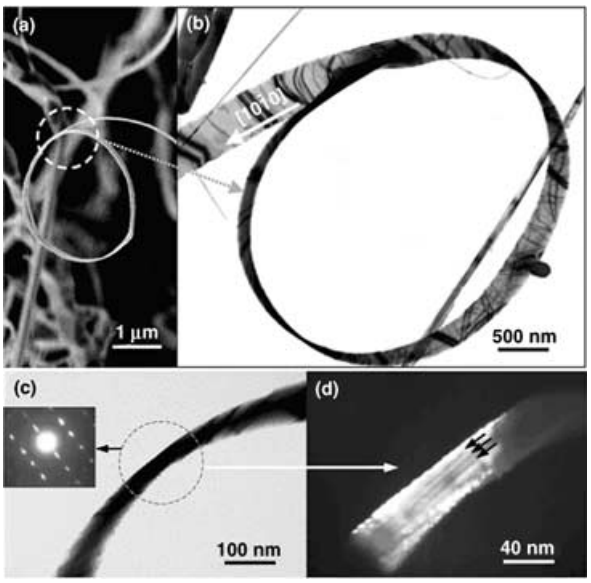

Figure 4. a) An SEM image showing a nanoloop, and b) a corresponding TEM image indicating that the nanobelt is dominated by {0001} polar surfaces and its growth direction is $[01\bar{1}0]$. c) Bright-field and d) corresponding dark-field TEM images recorded from a twist point of a polar nanobelt, which forms a nanospring, showing the presence of planar defects (marked by arrows) parallel to the large surface. The inset is an electron diffraction pattern recorded from the twisting area.

surfaces.[15] This result excludes the dominant effect of surface stress in the formation of nanoloops.

A spiral shape is also possible to reduce the electrostatic energy (Figure 3f), which is formed by a nanobelt whose thickness may increase slightly along its length. An in-plane spiral curling of the nanobelt tends to minimize the electrostatic energy between the ionic charges on the polar surfaces (Figure 3g).[22] If the distance between the loops is small, a densely packed spiral is formed (Figure 3h).

The key result presented in this paper is the high-yield synthesis of nanosprings, which makes possible their property characterization and application. The question to be answered is what is the key kinetic factor for the high-yield growth of nanosprings? It is a well-known fact that the {0001} polar surfaces are the dominant facets of single-crystal nanosprings and nanoloops of ZnO, and there is no doubt that the polar charges induce the formation of these unique structures.[7] Since the {0001} polar surfaces have higher surface energy than either $\{2\bar{1}\bar{1}0\}$ or $\{10\bar{1}0\}$, finding experimental conditions that make it possible for the formation of the higher-energy {0001} surface is the key. To find a clue, Table 1 summarizes the experimental conditions, growth morphology, and dominant surfaces of the ZnO nanostructures that we have synthesized using the same experimental setup during the last five years. The table clearly shows that, despite the source peak temperature in the range of 1300–1400 °C and a variation in vaporization time, both polar- and nonpolar-surface-dominated nanobelts could be produced. In the column of source materials used, it is clearly seen that polar-surface-dominated nanobelts were synthesized with or without doping of the ZnO. The

Table 1. A summary of the ZnO beltlike nanostructures synthesized by a solid–vapor process.

Nanostructures	Nanobelt growth direction; Dominant surfaces	Yield [%]	Peak temperature [°C]; Time at peak temperature [min]; Source materials	Ar flow rate [sccm]	Pre-growth pressure [mbar]; Pressure during growth [mbar]
Nanobelts [11]	[0001];{10$\bar{1}$0} or [10$\bar{1}$0];{2$\bar{1}\bar{1}$0}	100	1400; 120; ZnO	50	400; 400
Nanosprings and nanorings [13, 22]	[2$\bar{1}\bar{1}$0];{0001}	$\approx$5	1350; 30; ZnO:LiO_2	25	$\approx10^{-3}$; 330
Nanorings [14]	[10$\bar{1}$0];{0001}	$\approx$20	1400; 30; ZnO:In_2O_3:Li_2CO_3	50	$\approx10^{-3}$; 660
Nanobows [15, 23][a]	[10$\bar{1}$0];{0001}	5	1350; 120–600; ZnO	50	$\approx10^{-2}$; 300
Nanosprings (current work)	[2$\bar{1}\bar{1}$0];{0001}	50–100	1390; 120–360; ZnO	50	$\approx10^{-3}$; 250–300
Nanorings and nanosprings (current work)	[10$\bar{1}$0];{0001}	20	1390; 120–360; ZnO	50	$\approx10^{-3}$; 250–300

[a] The pressure in the growth chamber was quickly lowered to $\approx$0.1 mbar towards the end of the growth period.

gas flow pressure also appears not to be critical to the formation of polar surfaces unless the pressure becomes very low.[23] A common and striking fact is that a pre-evacuation of the growth chamber to $\approx10^{-3}$ mbar appears to be necessary for growing {0001}-dominated nanobelts. It is suggested that a pre-pumping would reduce the content of oxygen and other gas species in the growth chamber, thus, greatly reducing the possibility of molecular adsorption onto the {0001} polar surfaces. This step appears to be the key for high-yield growth of polar-surface-dominated nanostructures. In the current work, the synthesis was conducted at 1390 °C for $\approx$2–6 h under a confined pressure range of $\approx$250–300 mbar, which was applied after the temperature of the reaction chamber was ramped to 800 °C; the argon carrier gas flow rate was 50 sccm (standard cubic centimeters per minute) throughout the high-temperature synthesis and cooling processes. Before inletting the argon carrier gas, a pre-growth pressure of $\approx10^{-3}$ mbar was maintained for 3 to 8 h. In a separate experiment, we found that a sudden drop in chamber pressure can also lead to the formation of polar-surface-dominated nanobows.[23]

Structurally, we found that planar defects like stacking faults confined in the {0001} plane are present in the nanobelts dominated by {0001} facets. Figure 4c shows a bright-field TEM image recorded at the twisting point of a nanospring, in which the incident electron beam is parallel to the (0001) plane. A corresponding dark-field TEM image from the area (Figure 4d) clearly indicates the presence of planar defects (see the arrows). We know that planar defects lie in the {0001} plane and that they tend to lead to fast growth along the plane of the defects, making it possible to form {0001}-dominated nanobelts.[24] The driving force for this fast growth is unclear, but the planar defects are found to be the key in the growth of platelet nanocrystals.[25] It is possible that the presence of planar defects could lower, or overcome, the energy barrier required for growing the polar-surface-dominated nanostructures.

In summary, by controlling the growth kinetics through refining parameters such as temperature, pressure, and growth time, especially the pre-growth pressure level, single-crystal ZnO nanosprings were synthesized at high yield (>50 %). Our experiments indicate that doping is not necessary for forming polar-surface-dominated nanosprings and nanoloops, but a pre-growth low pressure seems to be the key. The nanobelts that form nanosprings grow along [2$\bar{1}\bar{1}$0], and the ones that form nanoloops/nanospirals grow along [10$\bar{1}$0]. It is suggested that planar defects are usually present in the polar-surface-dominated nanobelts. This work demonstrates that simple control of the pre-growth conditions results in a greatly improved yield of nanosprings. This study makes it possible to synthesize high purity nanosprings at high yield, opening the door to systematically understanding the properties and exploring the applications of semiconducting and piezoelectric nanosprings of ZnO.

Experimental Section

For the synthesis of ZnO nanosprings, a high-temperature, solid–vapor deposition process was used. The experimental setup consisted of a horizontal, alumina tube furnace, a rotary pump system, and a gas controlling system. Commercial ZnO powder (2 g, Alfa Aesar) was compacted and loaded on an alumina boat and positioned at the center of the alumina tube as the source material. The solid–vapor deposition was conducted at 1390 °C for $\approx$2–6 h under a confined pressure range of 250–300 mbar, which was applied after the temperature of the reaction chamber was ramped to 800 °C; argon carrier gas with a flow rate of 50 sccm was used throughout the high-temperature synthesis and cooling processes. The ramp rate was controlled at 25 °C min^{-1} in the temperature range from room temperature to 800 °C and at 20 °C min^{-1} from 800 °C to the deposition temperature (1390 °C). The as-grown nanosprings of ZnO were grown on a polycrystalline Al_2O_3 substrate in the temperature range of $\approx$500–600 °C.

Field-emission SEM (field-emission LEO 1530 FEG at 5 and 10 kV), TEM (field-emission TEM Hitachi HF-2000 at 200 kV), and energy-dispersive X-ray spectroscopy (EDS), attached to both the SEM and TEM instruments, were used to investigate the morphology, crystal structure, and composition of the as-grown nanostructures.

Keywords:
kinetics · nanosprings · polar surfaces · synthesis · zinc oxide

[1] Z. C. Jin, I. Hamberg, C. G. Granqvist, *J. Appl. Phys.* **1988**, *64*, 5117 – 5131.
[2] S. J. Pearton, C. R. Abernathy, M. E. Overberg, G. T. Thaler, D. P. Norton, N. Theodoropoulou, A. F. Hebard, Y. D. Park, F. Ren, J. Kim, L. A. Boatner, *J. Appl. Phys.* **2003**, *93*, 1 – 13.
[3] S. J. Pearton, D. P. Norton, K. Ip, Y. W. Heo, T. Steiner, *Prog. Mater. Sci.* **2005**, *50*, 293 – 340.
[4] A. H. Macdonald, P. Schiffer, N. Samarth, *Nat. Mater.* **2005**, *4*, 195 – 202.
[5] P. W. Tasker, *J. Phys. C: Solid State Phys.* **1979**, *12*, 4977 – 4984.
[6] Z. L. Wang, *J. Phys. Condens. Matter* **2004**, *16*, R829 – R858.
[7] Z. L. Wang, X. Y. Kong, Y. Ding, P. X. Gao, W. L. Hughes, R. S. Yang, Y. Zhang, *Adv. Funct. Mater.* **2004**, *14*, 944 – 956.
[8] Y. N. Xia, P. D. Yang, Y. G. Sun, Y. Y. Wu, B. Mayers, B. Gates, Y. D. Yin, F. Kim, Y. Q. Yan, *Adv. Mater.* **2003**, *15*, 353 – 389.
[9] M. H. Huang, S. Mao, H. Feick, H. Yan, Y. Wu, H. Kind, E. Weber, R. Russo, P. Yang, *Science* **2001**, *292*, 1897 – 1899.
[10] J. Zhang, L. D. Sun, C. S. Liao, C. H. Yan, *Chem. Commun.* **2002**, 262 – 263.
[11] Z. W. Pan, Z. R. Dai, Z. L. Wang, *Science* **2001**, *291*, 1947 – 1949.
[12] Z. L. Wang, X. Y. Kong, J. M. Zuo, *Phys. Rev. Lett.* **2003**, *91*, 185 502.
[13] X. Y. Kong, Z. L. Wang, *Nano Lett.* **2003**, *3*, 1625 – 1631.
[14] X. Y. Kong, Y. Ding, R. Yang, Z. L. Wang, *Science* **2004**, *303*, 1348 – 1351.
[15] W. Hughes, Z. L. Wang, *J. Am. Chem. Soc.* **2004**, *126*, 6703 – 6709.
[16] P. X. Gao, Z. L. Wang, *J. Appl. Phys.* **2005**, *97*, 044 304 – 044 310.
[17] P. X. Gao, Z. L. Wang, *J. Phys. Chem. B* **2002**, *106*, 12 653 – 12 658.
[18] J. Y. Lao, J. G. Wen, Z. F. Ren, *Nano Lett.* **2002**, *2*, 1287 – 1290.
[19] P. X. Gao, Z. L. Wang, *Appl. Phys. Lett.* **2004**, *84*, 2883 – 2885.
[20] Z. R. Tian, J. A. Voigt, J. Liu, B. Mckenzie, M. J. Mcdermott, M. A. Rodriguez, H. Konishi, H. Xu, *Nat. Mater.* **2003**, *2*, 821 – 826.
[21] F. Li, Y. Ding, P. X. Gao, X. Q. Xin, Z. L. Wang, *Angew. Chem.* **2004**, *116*, 5350 – 5354; *Angew. Chem. Int. Ed.* **2004**, *43*, 5238 – 5240.
[22] X. Y. Kong, Z. L. Wang, *Appl. Phys. Lett.* **2004**, *84*, 975 – 977.
[23] W. L. Hughes, Z. L. Wang, *Appl. Phys. Lett.* **2005**, *86*, 043 106 – 043 108.
[24] Y. Ding, X. Y. Kong, Z. L. Wang, *Phys. Rev. B* **2004**, *70*, 235 408.
[25] V. Germain, J. Li, D. Ingert, Z. L. Wang, M. P. Pileni, *J. Phys. Chem. B* **2003**, *107*, 8717 – 8720.

Received: May 13, 2005
Published online on July 8, 2005

